Back-Contacted GaInP/GaAs LED Structures by Ex-Situ Dopant Redistribution

Antti Myllynen, Seyed Ahmad Shahahmadi, Ivan Radevici, and Jani Oksanen

***Abstract*— Compound semiconductor devices utilizing interdigitated back-contact (IBC) designs with a uniform active region (AR) can enable a new generation of optoelectronic devices with eliminated contact shading, reduced resistive losses, and minimal current crowding. However, appropriate lateral doping techniques for such devices are not yet established. This work demonstrates selective-area diffusion doping from an epitaxially grown dopant source layer enabling the fabrication of GaAs-based light-emitting diodes (LEDs) utilizing diffusion-driven charge transport (DDCT) and the IBC design. The effects of doping and device dimensions are analyzed by comparing current–voltage characteristics and electroluminescence (EL) of laterally doped DDCT structures and control structures with several characteristic finger widths between 15 and 300 μm. Additional simulations confirm that the DDCT structure enables effective carrier injection into a buried AR outside the p-n junction. A current density of 1.25 A/cm^2 was measured for the fabricated DDCT-LED with 15-μm wide fingers at a moderate bias voltage of 1.3 V. The light emission from the DDCT-LEDs shows clear signs of lateral current injection, improved current spreading, and a tenfold increase in EL, when compared to control structures specifically designed to validate the presence of diffusion doping. These results indicate that diffusion doping can enable the means to fabricate DDCT structures with effective carrier injection into a uniform AR.**

***Index Terms*— III-arsenide, diffusion doping, diffusion-driven charge transport (DDCT), interdigitated back-contacted (IBC), light-emitting diode (LED).**

I. Introduction

DESPITE tremendous developments in compound semiconductor optoelectronics, the performance of conventional light-emitting diodes (LEDs) and solar cells, where the active region (AR) is sandwiched between the p-n junction, is still limited by resistive losses, current crowding [1], [2], and contact shading [3], [4]. Recent modeling works [5], [6], [7], [8], [9] have suggested that all of these issues could be minimized with laterally doped devices utilizing diffusion-driven charge transport (DDCT) [10] which enable single-sided current injection into ARs located outside the p-n junction. Furthermore, DDCT can facilitate, also for compound semiconductors, the well-known interdigitated back-contact (IBC) structure with uniform AR that provides the most efficient single-junction silicon solar cells [11]. With substrate removal, DDCT enables thin-film devices with near-surface AR and completely exposed front surface for efficient light extraction and absorption, enabling also, for example, three- and four-terminal multijunction devices [12], [13] fully based on III–V materials. As such, DDCT devices can reduce the energy consumption of general lighting, increase the energy yield of solar cells, and lead to new innovations in emerging fields such as optical cooling [14], [15], [16], [17] and waste heat harvesting through thermophotonics [18] and thermophotovoltaics [19], [20].

Fabrication of compound semiconductor-based DDCT devices is not established due to the unconventional device structures and lack of appropriate lateral doping techniques. So far, experimental studies on DDCT-LEDs have focused merely on GaN devices [10], [21], [22], [23], [24], while GaAs devices have been considered only theoretically [7], [8], [9]. The first report of GaN-based DDCT-LEDs by Riuttanen et al. [10] demonstrated the fundamental principle of DDCT by injecting holes into AR through an n-GaN layer. More recently, Kim et al. [22] proposed that n-contact of such structure could be placed directly on a thin i-GaN layer lowering the barrier for hole injection, while Lee et al. [24] suggested lowering the barrier with ion implantation. In this work, we demonstrate the fabrication of back-contacted GaInP/GaAs double-heterojunction LEDs, as considered in our previous modeling work [7], and use drift-diffusion simulations to show that extending the p-doped region over originally lightly n-doped layers can reduce the barrier for hole injection despite the presence of a lateral p-n junction in GaInP. These GaAs-based devices, illustrated in Fig. 1(a), are enabled by ex-situ dopant redistribution utilizing Zn diffusion from patterned p+-GaAs layer.

II. Experiments

Fig. 1(b) shows the epistructure used for DDCT and control structures, whose cross sections are illustrated in Fig. 1(c) and (d), respectively, grown on a p-GaAs substrate with metalorganic vapor phase epitaxy (MOVPE) at 604 °C.

Manuscript received 2 June 2023; revised 25 July 2023; accepted 31 July 2023. Date of publication 15 August 2023; date of current version 22 September 2023. This work was supported in part by the Academy of Finland under Grant 314458 and Grant 348754/Aeropolis. The review of this article was arranged by Editor J. D. Phillips. *(Corresponding author: Antti Myllynen.)*

The authors are with the Engineered Nanosystems Group, School of Science, Aalto University, 00076 Aalto, Finland (e-mail: antti.i.myllynen@aalto.fi).

Color versions of one or more figures in this article are available at https://doi.org/10.1109/TED.2023.3302272.

Digital Object Identifier 10.1109/TED.2023.3302272

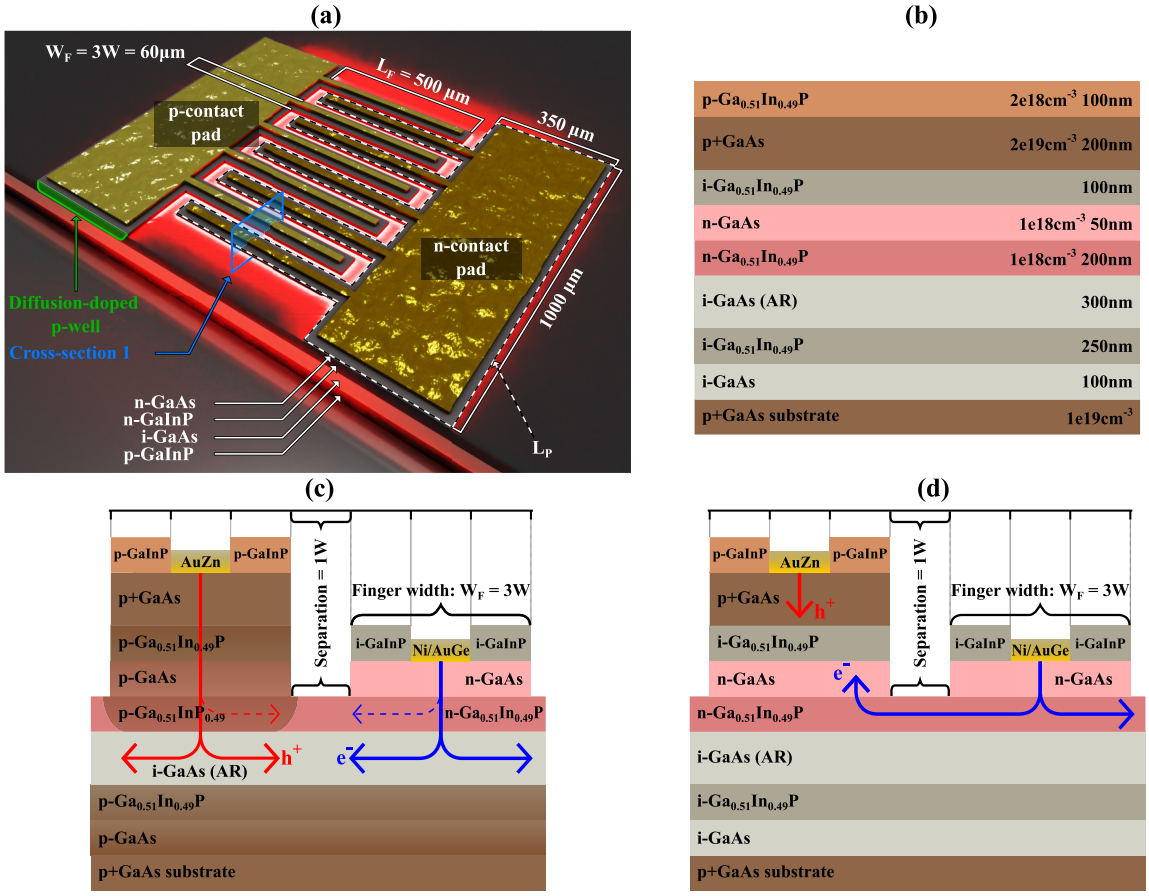

Fig. 1. (a) Concept picture of a thin-film DDCT-LED from the contact side after substrate removal. The green p-well highlights the diffusion-doped region under the p-mesa, while the blue square shows the cross section I, which is more closely illustrated in panels (c) and (d). (b) Epistructure as grown with MOVPE where i-layers are unintentionally doped with background carbon. (c) Cross section of diffusion annealed DDCT-LED where Zn has diffused toward i-GaAs AR from p+-GaAs layer and substrate. (d) Cross section of control structure without diffusion annealing having an otherwise identical design with the DDCT-LED. Electron (blue) and hole (red) current paths are illustrated for the dominating current (solid line) into AR and leakage current (dashed line) through the lateral p-n junction in the GaInP layer.

The control structure is specifically designed to validate the presence of diffusion doping in the DDCT structures: the p-n junction of the control structure is completely misaligned with the AR, and the only way to transform the control device into a properly working LED is by redistributing the highly diffusive Zn dopants to form a laterally doped DDCT device studied in [7] and [8]. The fabrication process for the devices is almost identical and differs only in the silicon nitride encapsulation and diffusion annealing which are only performed on the DDCT structures.

First, a 300-nm-thick p-mesa, consisting of p-GaInP and p+-GaAs top layers, is defined using an MLA-150 maskless aligner from Heidelberg with 405-nm laser exposure of photoresist (AZ5214E) and selective wet etching. To protect the surface of DDCT samples during diffusion annealing, 120 nm of silicon nitride (Si_3N_4) is deposited on both sides of the samples with plasma-enhanced chemical vapor deposition (PECVD) at 300 °C. Then, DDCT samples are placed between two pieces of silicon wafer and inserted into an open quartz tube furnace at room temperature before switching on the heater elements of the furnace. This provides a slow heating rate of ~20 °C/min which should minimize thermal stress that could lead to cracking of the Si_3N_4 film. Diffusion annealing is performed for 4 h at 650 °C with N_2 flow allowing diffusion of Zn from p+-GaAs and the substrate toward the AR. After annealing, the Si_3N_4 layer is removed with a buffered oxide etch (BOE), and n-mesas are formed with lithography and wet etching of the sacrificial i-GaInP and n-GaAs layers. Contact openings on DDCT and control samples are defined in the GaInP layers on top of both mesas so that the uncontacted areas remain covered by GaInP. Electron beam evaporation and metal lift-off are used to form AuZn/Zn/AuZn p-contacts and Ni/AuGe n-contacts that are annealed with rapid thermal annealing for 15 s at 300 °C with N_2 flow. This provides Ohmic contacts with specific contact resistivity of $4.5 \times 10^{-6}\ \Omega \cdot \mathrm{cm}^2$ for n-contact and $3.4 \times 10^{-5}\ \Omega \cdot \mathrm{cm}^2$ for p-contact as measured with the transfer length method (TLM) on contact test structures located elsewhere on the same sample.

Table I shows the most important dimensions of the studied devices. Linewidth (W) is the minimum linewidth reached in the fabrication process ranging from 5 to 100 μm, which also corresponds to the distance between adjacent fingers and the separation between contact and mesa edges. The n- and p-fingers have a characteristic finger width (W_F) of $3W$ which is also used for naming the devices as, for

TABLE I

LINEWIDTH (W), CHARACTERISTIC FINGER WIDTH (W_F), NUMBER OF FINGERS (N), MESA PERIMETER LENGTH (L_P), AND AREA (A) OF THE STUDIED DEVICES. THE INTERNAL SERIES RESISTANCE (R_s) IS CALCULATED FOR DDCT-LEDS ONLY

Device	W (μm)	W_F (μm)	N	L_P (cm)	R_s (Ω)
DDCT-15 & Control-15	5	15	24	2.67	8.50
DDCT-30 & Control-30	10	30	11	1.17	10.0
DDCT-60 & Control-60	20	60	5	0.5	13.8
DDCT-300 & Control-300	100	300	1	0.1	144

example, DDCT-15 and Control-15 for DDCT and control structures with $W_F = 15$ μm, respectively. As W_F decreases the number of fingers (N) increases the contact mesa sidewall perimeter length (L_P) which can substantially affect the nonradiative recombination at the surface [1] if it is accessible to the carriers either through leakage or unoptimal placement of the p-n junction. The length of the fingers (L_F) is 500 μm and the separation between the end of the p-fingers and the n-contact pad is $2W$. The active device area used to calculate the average current densities through the devices is defined as the area of the p-mesa including the contact pad (1000 μm $\times$ 350 μm) and the area of the fingers calculated as $W_F \times N \times L_F$, which is slightly different for each device. Overall, the lateral dimensions of the studied devices here are similar to the recently reported GaN-based DDCT-LEDs [22].

The current–voltage (J–V) characteristics of the fabricated devices are measured using a two-wire setup with a Keithley 2612b as the voltage source with continuous current injection. The electroluminescence (EL) from the devices is captured with a Flame-S-CR1-ES spectrometer and a QP600-1-VIS-NIR optical fiber from Ocean Optics using pulsed current injection ensuring minimal heating of the device. The optical fiber is pointed at the middle of the finger array on the contact side of the LEDs. Additionally, a standard CMOS camera (350–1000 nm) is used to image the spatial distribution of light emission in the devices.

III. DEVICE MODELING

The theoretical foundations of the devices are studied with drift-diffusion simulations coupling the partial differential equations for the quasi-Fermi levels of electrons and holes and the electrostatic potential in the 2-D real space. Due to the periodic nature and symmetry of the finger structures, the simulated region of the devices extends from the middle of the p-contact to the middle of the n-contact in the lateral dimension in Fig. 1(c) and (d) and excludes the contact pads and the thick-substrate region for simplicity. A more detailed description of the model can be found in, for example, [7], [8].

The expected physical changes induced by the diffusion doping are easiest to describe by comparing the cross section of DDCT and control structures illustrated in Fig. 1(c) and (d), respectively. In DDCT devices, Zn diffusion extends the p-doped region over the originally lightly doped n-layers and enables injection of holes (red dashed arrows) and electrons (blue arrows) into the buried unintentionally doped i-GaAs AR through the respective laterally doped

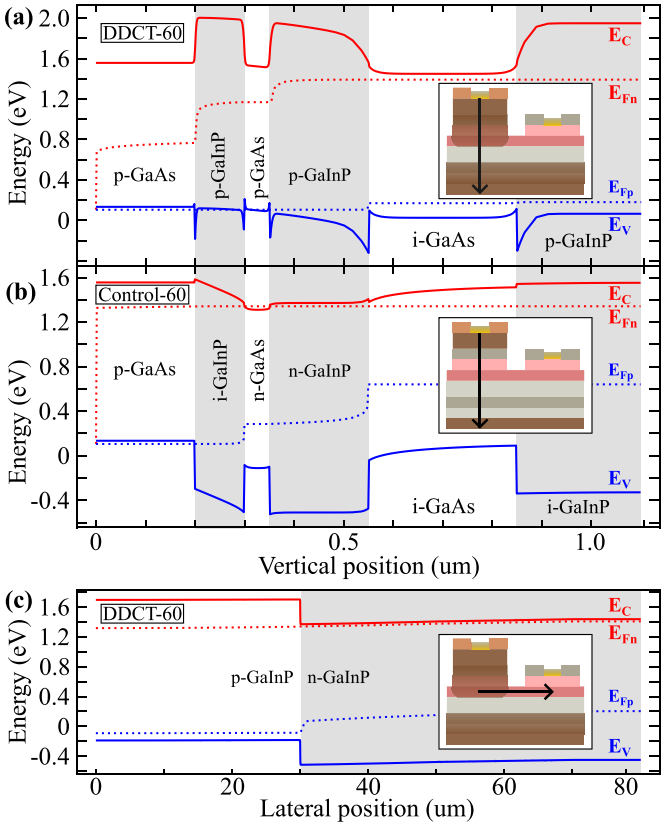

Fig. 2. Energy band diagrams for selected devices at 1.3 V along the paths illustrated in each inset. Band diagrams of (a) DDCT-60 and (b) Control-60 show that hole injection into the AR is only possible in the DDCT-60 device because the large valence band potential barriers in Control-60 block it. (c) Lateral p-n junction within the diffusion-doped GaInP layer in DDCT-60 forms a large barrier in E_C and E_V blocking most of the current transport across the GaInP junction. More detailed layer structures of the insets are shown in Fig. 1, with the p-doping in the second p-GaInP layer in panel (a) assumed to decrease toward the AR to resemble a typical diffusion doping profile more closely.

finger regions. This behavior is also observed in Fig. 2(a) showing the calculated energy band diagram of DDCT-60 at 1.3 V along the path shown in the inset. Although some narrow potential barriers are still present due to valence band offsets, holes can be efficiently injected into the i-GaAs AR. In contrast, similar data for Control-60 in Fig. 2(b) shows that hole injection into the AR is blocked by the high potential barriers induced by the n-GaAs and n-GaInP layers. In this sense, the control structure resembles the previously reported GaN DDCT-LED structures [10].

In the lateral direction, the energy band diagram across the p-GaInP/n-GaInP junction in Fig. 2(c) shows ~300-meV barriers in conduction and valence bands for the DDCT-60 structure even at 1.3 V suggesting that the leakage current across the lateral GaInP junction is negligible at moderate biases. Therefore, conventional device mesas, exposing the edges of the AR, are not needed. Instead, the effective device area is limited by the size of the contact array which can facilitate the development of large-area devices utilizing even the whole substrate area. This is possible with, for example, a multilevel point contact design extending throughout the substrate. Additionally, since device mesas are not needed, the

surface recombination at the edges of the AR located far from the contact array is practically eliminated [7]. Although the design of the control sample is suboptimal, it is the appropriate structure for sensing the improvements achieved by diffusion annealing. For this reason, DDCT and control samples are processed simultaneously, whenever possible, on different quarters of the same wafer. Therefore, all major differences between the device structures and performance should be caused by the diffusion doping and Si_3N_4 encapsulation, performed only on the DDCT samples.

IV. Results and Discussion

A. Electrical Properties

The effect of diffusion doping on device performance is studied by directly comparing the J–V characteristics of the DDCT structures to those of the control structures. To provide a baseline level for a typical J–V response of a GaInP/GaAs double heterojunction, we also include data for a LED structure of the double diode structure used in [17]. The resulting J–V data is shown in Fig. 3. The DDCT devices exhibit a typical LED behavior with an exponentially increasing current at small voltages and current saturation due to internal resistance at larger voltages. The linear region below 1 V of the device DDCT-300 corresponds to a Shockley-Read-Hall (SRH) recombination-dominated region with a reasonable saturation current density ($J_{0,n=2}$) in the order of $\sim 2 \times 10^{-11}$ A/cm^2. With smaller W_F, $J_{0,n=2}$ is only marginally worse when compared to DDCT-300. Furthermore, the saturation current density of DDCT devices is lower than for the reference LED that has $J_{0,n=2}$ of $\sim 6 \times 10^{-10}$ A/cm^2. Overall, the values of $J_{0,n=2}$ show that diffusion annealing at 650 °C is unlikely to notably deteriorate the material quality, even though additional leakage current is observed for DDCT-15, DDCT-30, and DDCT-60 at V < 0.7 V. This indicates that the increased L_P might lead to additional surface channels and recombination at the sidewalls of p-mesa. Furthermore, the contribution of these channels can increase as W and consequently, the distance between the metal contact and the mesa edge is reduced.

The lateral dimensions are also clearly reflected on the internal series resistance (R_s) shown in Table I for the DDCT devices when neglecting $R_s = 3.75$ Ω of the measurement system. The amount of R_s increases with W which is reasonable since W also corresponds to the distance between the p- and n-mesa, and 3 W corresponds to the full distance carriers need to diffuse to produce fully uniform luminescence distribution. When extrapolating R_s for devices with W_F <15 μm, the resistance minimizes at approximately 7 Ω, indicating that the lateral distance between adjacent fingers is not the only factor contributing to R_s. We estimate that part of the resistance is likely to originate from the 500-μm-long relatively thin metal contact fingers and potentially the p-GaInP layer of the p-mesa which can introduce an additional potential barrier for holes.

While similar trends are observed for the control structures, they have several orders of magnitude higher shunt-like leakage current when compared to the DDCT devices. This indicates that the charge carriers must be leaking through

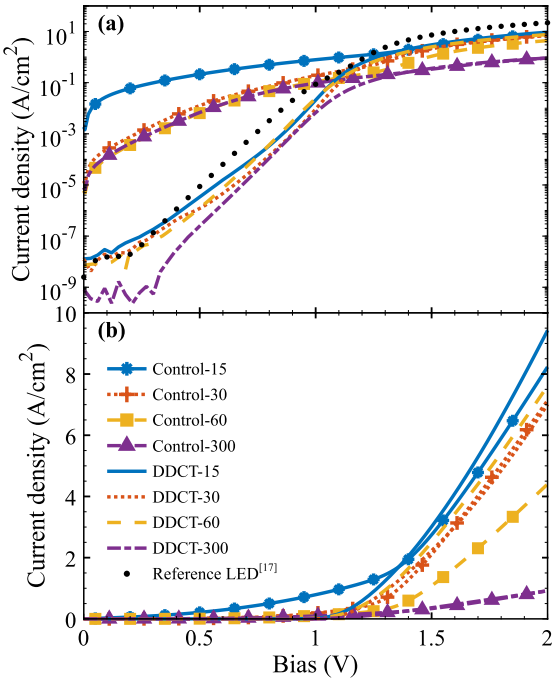

Fig. 3. Effects of lateral doping are reflected in the J–V characteristics of the structures plotted on (a) logarithmic and (b) linear y-axis, showing significantly lower leakage currents for the DDCT structures. However, DDCT and control devices show significantly higher series resistance when compared to the reference LED.

or across the i-GaInP layer, separating the p+-GaAs and n-GaAs layers within the p-mesa, and recombining in these GaAs layers having a huge surface recombination velocity of $\sim 10^6$ cm/s [25]. We estimate that a significant part of the leakage current leads to nonradiative surface recombination which is a typical problem of conventional flip-chip LEDs [26] that can be extremely severe in devices with large L_P [1]. The charge transport in the DDCT-LEDs is quite different since the location of the primary p-n junction has shifted into the originally n-doped GaInP cladding layer or the AR during the diffusion annealing. Because of the depletion region of the shifted junction, the minority carrier density in the p-mesa becomes very small and the surface recombination rate at the sidewalls is minimized. Therefore, even if the hole current would leak along mesa edges, the effect on device performance would be minimal in the DDCT devices. Overall, the general trends observed for the fabricated devices agree with our previous modeling work [7] which showed practically eliminated surface recombination rate for DDCT-LEDs, higher current density at high biases for the devices with the smallest finger width, but also higher leakage current at low voltages due to increased depletion region volume.

The observations made from the J–V curves are supported by simulated current density $\vec{J} = \vec{J}_x + \vec{J}_y$ of DDCT-60 and Control-60 shown in Fig. 4. Fig. 4(a) shows that current distribution in DDCT-60 is significantly more even when compared to Control-60 in Fig. 4(b), as current is clearly injected into the AR and even the bottom p-GaInP layer contributing to the current spreading in the lateral direction. In contrast, since effective current injection into the AR is not possible in the Control-60, the current density becomes very high in the n-GaAs layer. Because the n-GaAs is directly

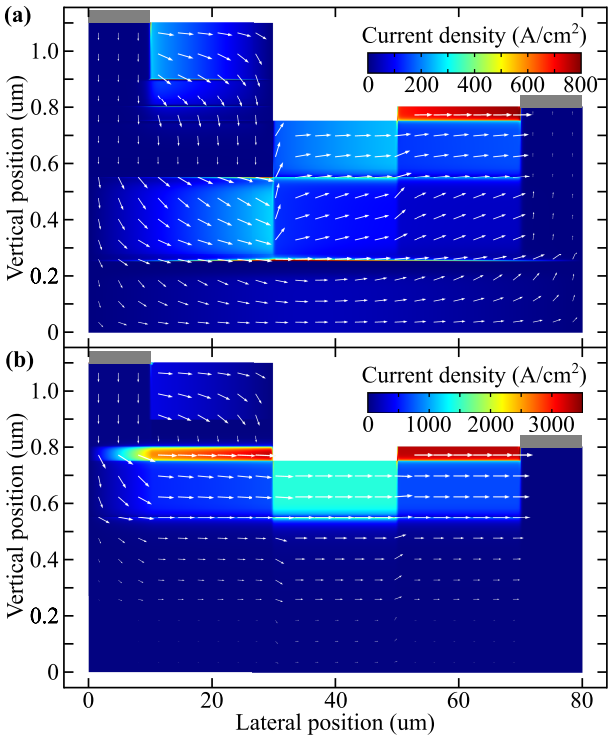

Fig. 4. Magnitude and direction of the current density $\vec{J}$ for (a) DDCT-60 and (b) Control-60 at 1.3 V. The current distribution is more uniform in DDCT-60, where significant currents are also injected into the AR. In contrast, strong currents cannot be injected into the AR in Control-60 due to the potential barriers, leading to very high current density within the n-GaAs and n-GaInP layers close to the exposed GaAs surface. The perceived discontinuities in the current densities are due to the different dimensions and scaling of the figure in lateral and vertical directions and indicate simply the redistribution of the current into different material layers.

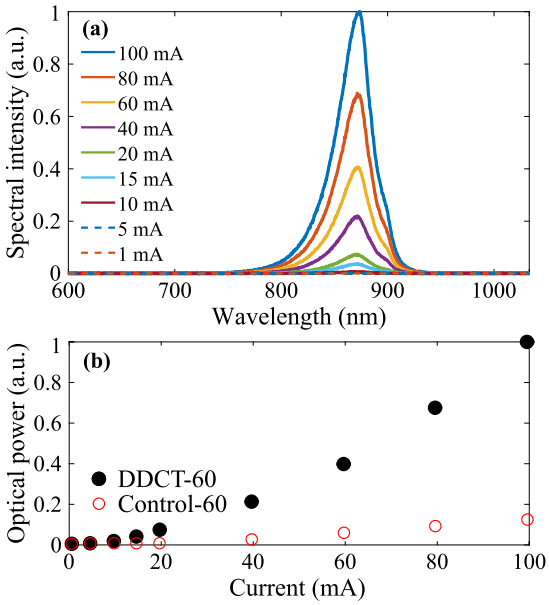

Fig. 5. (a) Emission spectra of DDCT-60 at different injection currents. (b) Comparison of optical power between DDCT-60 and Control-60 at different injection currents showing a tenfold increase in brightness for the DDCT device.

exposed to air, this leads to an increased surface recombination rate at the exposed mesa edge, as indicated by the pronounced leakage currents in the control devices in Fig. 3. While some current flows through the AR of the control structure, it fully consists of electron current, and therefore, not leading to major recombination due to the lack of holes. Furthermore, the implications of the lateral GaInP junction are visible in Fig. 4(a) where the current bypasses the lateral p-n junction via the AR as indicated by the arrows.

B. Optical Properties

In addition to J–V characteristics, the EL and optical power (P_{out}) of the finger structures is analyzed. Fig. 5(a) shows the emission spectra of DDCT-60 for different input currents (I_{in}) with a peak at approximately 872 nm corresponding to the GaAs bandgap energy of 1.42 eV with no signs of GaInP emission around 690 nm (∼1.8 eV) even at a bias of 2 V. The full-width half-maximum (FWHM) of the spectra was approximately 36 nm at $I_{\text{in}} = 20$ mA showing slightly higher values at higher I_{in}. The change in FWHM is caused by a weak additional peak around 900 nm which is stronger at higher I_{in} broadening the main peak. This additional peak can be caused by a few reasons. First, the peak can originate from Ga or As vacancies [27] that can form during diffusion annealing, but this is unlikely since a similar peak was also observed for the control structures. Second, the additional peak can be emitted from the p-doped GaAs layers [28] located within the p-mesa. Data from all device sizes (not shown here) support the latter possibility since the 900-nm peak is more pronounced in devices with large W_F, indicating that it is most likely originating from the p-mesa. One explanation for such behavior is the limited current spreading capabilities of, for example, DDCT-300 due to the large distance between adjacent fingers. This can lead to conventional current crowding where most of the light is emitted near the p-contact edge inside the p-mesa. Therefore, we expect that the contribution of the 900-nm peak reduces with W_F due to the improved current spreading capabilities of narrow fingers. Fig. 5(b) compares P_{out} of DDCT-60 and Control-60 normalized by the power of the DDCT-LED at $I_{\text{in}} = 100$ mA. The radiance measured from the contact side shows a tenfold increase in light emission from the DDCT-60 with $I_{\text{in}} \geq 10$ mA. This indicates that the diffusion doping has indeed been sufficient to shift the junction position in DDCT devices enabling efficient hole injection into the buried AR. However, the exact location of the Zn diffusion front or the doping profile has not been measured. The weaker P_{out} of the Control-60 supports the observations made from the J–V curves and the device simulations indicating severe nonradiative recombination at the mesa edge.

The current spreading capabilities of the structures are compared by analyzing the spatial distribution of light emission captured from the contact side. Fig. 6(a) and (b) shows the light emission at $I_{\text{in}} = 20$ mA for the DDCT-60 and Control-60, respectively. Despite the limited resolution of the camera, Fig. 6 enables confirming the main features and differences in the carrier spreading. In both devices, most of the light is emitted from the area defined by the p-mesa fingers due to the still relatively long distance between n- and p-contacts. While the exact layer where the radiative

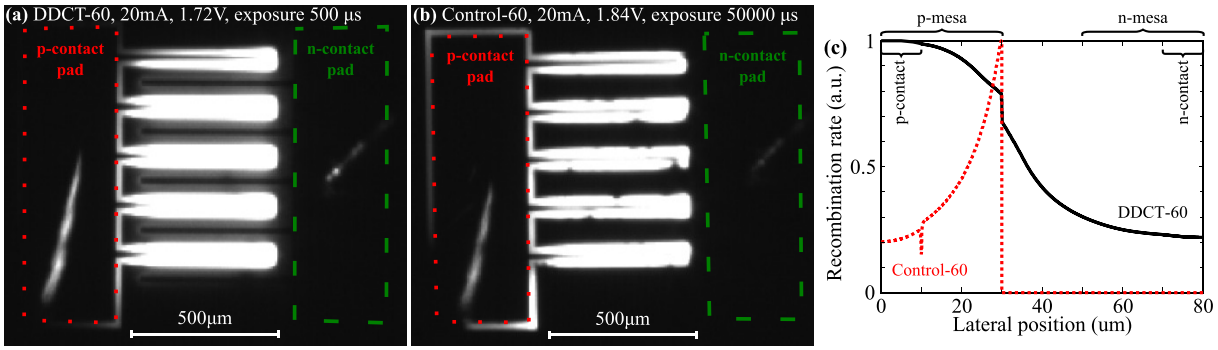

Fig. 6. EL at an input current of 20 mA from devices (a) DDCT-60 and (b) Control-60 shows a clear difference, especially under the n-fingers. (c) Simulated recombination profiles show strong current spreading toward the n-mesa for the DDCT-60, while in Control-60, recombination is strongly focused under the p-mesa. Panels (a) and (b) are slightly overexposed on purpose to highlight the differences, and panel (c) is normalized to enable easier comparison between the devices.

recombination occurs is impossible to identify from these figures, Fig. 6(a) clearly shows that light is emitted also under the n-mesa area of the DDCT device. This is evident by the n-contact metal finger being visible as a dark line since it blocks the light emitted under the n-mesa. Fig. 6(b) shows no emission for the Control-60 between the bright p-fingers even though the camera exposure time is 100 times longer. This is true also with lower and higher I_{in} and even when increasing the exposure time.

The simulated recombination profiles of DDCT-60 and Control-60 in Fig. 6(c), calculated from the total recombination rates, including radiative, SRH, Auger, surface, and interface recombination processes, support the observations made above by showing strong current spreading toward the n-mesa only for the DDCT device. In contrast, Control-60 shows a different profile where recombination is focused under the p-mesa. The overall trends of the simulation results in Fig. 6(c) agree well with the experimental data, and the current spreading of DDCT-60 is only ∼30% stronger in the simulations when compared to the experimental measurements despite the simulations being 2-D and not fully calibrated for all the device parameters. Alternatively, light emission can originate from the n- and p+-GaAs layers as suggested by the EL spectra. However, emission from the n-GaAs contact layer seems unlikely due to the layer design and a lack of a darker region that should be visible between the mesa fingers where the n-GaAs layer has been removed. Also, the contribution of p+-GaAs is estimated to be minimal as suggested by the spectra. Together, the simulations, the spectra in Fig. 5(a) showing emission only from GaAs, and the spatial distribution of EL suggest that the light is emitted from the uniform i-GaAs layer of the DDCT-LED, which is a clear sign of diffusion-driven carrier injection into the buried AR.

C. Discussion

While the design and fabrication process of the current DDCT structures is not fully optimized, the results largely confirm the previous predictions that back-contacted devices having all contacts on the same side of the AR are possible also for the GaAs-based materials. In particular, devices with small W_F provide better current spreading within the AR and exhibit lower internal resistance in line with expectations [7]. This is partly due to the currently used symmetrical lateral structure, in which n- and p-fingers have identical widths, diffusion still needs to transport the carriers over relatively large distances, meaning that these structures cannot completely reach the region of ideal operation with uniform light emission and eliminated resistance related to current spreading. Therefore, the width of the n-finger should be reduced further in the next-generation fabrication processes to counterbalance the significantly lower hole mobility in GaAs. This requires some process optimization since the linewidth of the fabrication process is currently limited to ∼5 μm due to undercut during GaInP wet etching. As such, the present work also illustrates the general challenges that other laterally injected devices, such as electrically pumped nanocavity lasers [29], are facing. Furthermore, to unlock the true potential of DDCT devices including near-surface AR and surface modifications, the contact side should be designed to be highly reflective with, for example, omnidirectional reflectors, and the substrate should be removed by etching or epitaxial lift-off.

V. Conclusion

In conclusion, this work demonstrates that ex-situ diffusion of dopants incorporated in epitaxially grown source layers can facilitate the fabrication of GaAs-based DDCT-LEDs that can enable IBC designs for III–V materials. Current–voltage characteristics show that effective carrier injection is possible at a moderate bias of 1.3 V resulting in a current density of 1.25 A/cm^2 in devices with 15-μm finger width. Also, saturation current density $J_{0,n=2}$ in the order of 2×10^{-11} A/cm^2 suggests that good material quality can be maintained even in diffusion-doped samples. Emission spectra of the DDCT device show a strong peak at 872 nm corresponding to the bandgap energy of 1.42 eV of the i-GaAs AR. These results suggest that electrical excitation of the buried AR is possible through the laterally doped contact finger array. Consequently, since the effective area of the DDCT devices is defined by the size of the contact array, conventional device mesas are not needed. Therefore, the free surfaces and surface recombination are practically eliminated from the AR. Overall, this work lays the foundation for the

future development of back-contacted large-area GaAs-LEDs and solar cells.

Acknowledgment

The authors would like to thank the provision of facilities and technical support by Aalto University at OtaNano–Micronova Nanofabrication Centre.

References

[1] X. Guo, Y.-L. Li, and E. F. Schubert, "Efficiency of GaN/InGaN light-emitting diodes with interdigitated mesa geometry," *Appl. Phys. Lett.*, vol. 79, no. 13, pp. 1936–1938, Sep. 2001, doi: 10.1063/1.1405145.

[2] A. V. Zinovchuk, O. Y. Malyutenko, V. K. Malyutenko, A. D. Podoltsev, and A. A. Vilisov, "The effect of current crowding on the heat and light pattern in high-power AlGaAs light emitting diodes," *J. Appl. Phys.*, vol. 104, no. 3, Aug. 2008, Art. no. 033115, doi: 10.1063/1.2968220.

[3] M. Steiner, S. P. Philipps, M. Hermle, A. W. Bett, and F. Dimroth, "Validated front contact grid simulation for GaAs solar cells under concentrated sunlight," *Prog. Photovolt., Res. Appl.*, vol. 19, no. 1, pp. 73–83, Jan. 2011, doi: 10.1002/pip.989.

[4] X. Wang, M. R. Khan, J. L. Gray, M. A. Alam, and M. S. Lundstrom, "Design of GaAs solar cells operating close to the Shockley–Queisser limit," *IEEE J. Photovolt.*, vol. 3, no. 2, pp. 737–744, Apr. 2013, doi: 10.1109/JPHOTOV.2013.2241594.

[5] P. Kivisaari, I. Kim, S. Suihkonen, and J. Oksanen, "Elimination of resistive losses in large-area LEDs by new diffusion-driven devices," *Proc. SPIE*, vol. 10124, Feb. 2017, Art. no. 101240Z, doi: 10.1117/12.2251108.

[6] P. Kivisaari, I. Kim, S. Suihkonen, and J. Oksanen, "Elimination of lateral resistance and current crowding in large-area LEDs by composition grading and diffusion-driven charge transport," *Adv. Electron. Mater.*, vol. 3, no. 6, May 2017, Art. no. 1700103, doi: 10.1002/aelm.201700103.

[7] A. Myllynen, T. Sadi, and J. Oksanen, "Current spreading in back-contacted GaInP/GaAs light-emitting diodes," *IEEE Trans. Electron Devices*, vol. 67, no. 3, pp. 1027–1033, Mar. 2020, doi: 10.1109/TED.2020.2964662.

[8] A. Myllynen, T. Sadi, and J. Oksanen, "Interdigitated back-contact double-heterojunction GaInP/GaAs solar cells," *Prog. Photovolt., Res. Appl.*, vol. 29, no. 1, pp. 47–53, Jan. 2021, doi: 10.1002/pip.3339.

[9] J. E. O'Connor and S. Michael, "Optimizing a single-absorption-layer thin-film solar cell[1] model to achieve 31% efficiency," *J. Mater. Sci. Chem. Eng.*, vol. 5, no. 1, pp. 54–60, 2017, doi: 10.4236/msce.2017.51008.

[10] L. Riuttanen et al., "Diffusion injected multi-quantum well light-emitting diode structure," *Appl. Phys. Lett.*, vol. 104, no. 8, Feb. 2014, Art. no. 081102, doi: 10.1063/1.4866343.

[11] K. Yoshikawa et al., "Silicon heterojunction solar cell with interdigitated back contacts for a photoconversion efficiency over 26%," *Nature Energy*, vol. 2, no. 5, Mar. 2017, Art. no. 17032, doi: 10.1038/nenergy.2017.32.

[12] E. L. Warren et al., "A taxonomy for three-terminal tandem solar cells," *ACS Energy Lett.*, vol. 5, no. 4, pp. 1233–1242, Mar. 2020, doi: 10.1021/acsenergylett.0c00068.

[13] R. C. Whitehead et al., "Optimization of four terminal rear heterojunction GaAs on Si interdigitated back contact tandem solar cells," *Appl. Phys. Lett.*, vol. 118, no. 18, May 2021, Art. no. 183902, doi: 10.1063/5.0049097.

[14] T. Sadi, I. Radevici, and J. Oksanen, "Thermophotonic cooling with light-emitting diodes," *Nature Photon.*, vol. 14, no. 4, pp. 205–214, Mar. 2020, doi: 10.1038/s41566-020-0600-6.

[15] T. Sadi, I. Radevici, P. Kivisaari, and J. Oksanen, "Electroluminescent cooling in III–V intracavity diodes: Practical requirements," *IEEE Trans. Electron Devices*, vol. 66, no. 2, pp. 963–968, Feb. 2019, doi: 10.1109/TED.2018.2885267.

[16] T. Sadi, I. Radevici, P. Kivisaari, and J. Oksanen, "Electroluminescent cooling in III–V intracavity diodes: Efficiency bottlenecks," *IEEE Trans. Electron Devices*, vol. 66, no. 6, pp. 2651–2656, Jun. 2019, doi: 10.1109/TED.2019.2910219.

[17] I. Radevici et al., "Thermophotonic cooling in GaAs based light emitters," *Appl. Phys. Lett.*, vol. 114, no. 5, Feb. 2019, Art. no. 051101, doi: 10.1063/1.5064786.

[18] T. Sadi, I. Radevici, B. Behaghel, and J. Oksanen, "Prospects and requirements for thermophotonic waste heat energy harvesting," *Sol. Energy Mater. Sol. Cells*, vol. 239, Jun. 2022, Art. no. 111635, doi: 10.1016/j.solmat.2022.111635.

[19] J. Song, M. Choi, Z. Yang, J. Lee, and B. J. Lee, "A multi-junction-based near-field solar thermophotovoltaic system with a graphite intermediate structure," *Appl. Phys. Lett.*, vol. 121, no. 16, Oct. 2022, Art. no. 163503, doi: 10.1063/5.0115007.

[20] A. LaPotin et al., "Thermophotovoltaic efficiency of 40%," *Nature*, vol. 604, no. 7905, pp. 287–291, Apr. 2022, doi: 10.1038/s41586-022-04473-y.

[21] L. Riuttanen, P. Kivisaari, O. Svensk, J. Oksanen, and S. Suihkonen, "Diffusion injection in a buried multiquantum well light-emitting diode structure," *IEEE Trans. Electron Devices*, vol. 62, no. 3, pp. 902–908, Mar. 2015, doi: 10.1109/TED.2015.2391117.

[22] I. Kim, C. Kauppinen, I. Radevici, P. Kivisaari, and J. Oksanen, "Back-contacted carrier injection for scalable GaN light emitters," *Phys. Status Solidi (A)*, vol. 219, no. 2, Jan. 2022, Art. no. 2100461, doi: 10.1002/pssa.202100461.

[23] M.-L. Lee, S.-S. Wang, Y.-H. Yeh, P.-H. Liao, and J.-K. Sheu, "Light-emitting diodes with surface gallium nitride p-n homojunction structure formed by selective area regrowth," *Sci. Rep.*, vol. 9, no. 1, p. 3243, Mar. 2019, doi: 10.1038/s41598-019-40095-7.

[24] M.-L. Lee, Y.-H. Yeh, Z.-Y. Liu, K.-J. Chiang, and J.-K. Sheu, "Planar GaN-based blue light-emitting diodes with surface p-n junction formed by selective-area Si–Ion implantation," *IEEE Trans. Electron Devices*, vol. 64, no. 10, pp. 4156–4160, Oct. 2017, doi: 10.1109/TED.2017.2738058.

[25] L. Pavesi and M. Guzzi, "Photoluminescence of $Al_xGa_{1-x}As$ alloys," *J. Appl. Phys.*, vol. 75, no. 10, pp. 4779–4842, May 1994, doi: 10.1063/1.355769.

[26] S. S. Konoplev, K. A. Bulashevich, and S. Y. Karpov, "From large-size to micro-LEDs: Scaling trends revealed by modeling," *Phys. Status Solidi (A)*, vol. 215, no. 10, May 2018, Art. no. 1700508, doi: 10.1002/pssa.201700508.

[27] A. Jorio, A. Wang, M. Parenteau, C. Carlone, N. L. Rowell, and S. M. Khanna, "Optical identification of the gallium vacancy in neutron-irradiated gallium arsenide," *Phys. Rev. B, Condens. Matter*, vol. 50, no. 3, pp. 1557–1566, Jul. 1994, doi: 10.1103/PhysRevB.50.1557.

[28] B. Tuck, "Photoluminescence of compensated p-type GaAs," *J. Phys. Chem. Solids*, vol. 28, no. 11, pp. 2161–2168, Nov. 1967, doi: 10.1016/0022-3697(67)90240-5.

[29] B. Ellis et al., "Ultralow-threshold electrically pumped quantum-dot photonic-crystal nanocavity laser," *Nature Photon.*, vol. 5, no. 5, pp. 297–300, Apr. 2011, doi: 10.1038/NPHOTON.2011.51.